Multi-parameter estimation of high-Q silicon rich nitride resonators using optical frequency domain reflectometry

Downloaded from: https://research.chalmers.se, 2024-04-24 09:57 UTC

Citation for the original published paper (version of record):

Bru, L., Ye, Z., Pastor, D. et al (2018). Multi-parameter estimation of high-Q silicon rich nitride resonators using optical frequency
domain reflectometry. Proceedings of SPIE - The International Society for Optical Engineering, 10535. http://dx.doi.org/10.1117/12.2290641

N.B. When citing this work, cite the original published paper.

research.chalmers.se offers the possibility of retrieving research publications produced at Chalmers University of Technology.
It covers all kind of research output: articles, dissertations, conference papers, reports etc. since 2004.
research.chalmers.se is administrated and maintained by Chalmers Library

(article starts on next page)

Multi-parameter estimation of high-Q silicon rich nitride resonators using optical frequency domain reflectometry

Luis A. Bru[a], Zhichao Ye[b], Daniel Pastor[a], and Pascual Muñoz[a]

[a]Photonics Research Labs, Universitat Politècnica de València, c/ Camino de Vera s/n, 46021 Valencia, Spain

[b]Department of Microtechnology and Nanoscience (MC2), Chalmers University of Technology, 41296 Gothenburg, Sweden

ABSTRACT

Many linear and nonlinear optics applications rely on micro-resonators (MRRs) with carefully designed dispersion and coupling rate coefficients. These parameters are however challenging to measure for MRRs based on high-confinement optical waveguides. In this paper, we report on the use of optical frequency domain reflectometry (OFDR) for the measurement of group velocity dispersion (GVD), coupling coefficients and round-trip loss, in high-Q ($Q_i \sim 0.3 \times 10^6$) silicon-rich nitride MRRs. This technique allows for retrieving the GVD coefficient, intrinsic losses and coupling coefficient for each transverse mode in the resonator, thus providing very valuable feed-back information from experiments to the design flow step.

Keywords: OFDR, high-Q microring resonator, interferometry, frequency comb, optical metrology, integrated photonics, group velocity dispersion, time domain response

1. INTRODUCTION

High-Q microring resonators (MRRs) are essential for frequency combs generation,[1] optical clocks[2] and high-precision sensing.[3] In this context, group velocity dispersion (GVD) is a critical design parameter as it influences the four-wave mixing efficiency in the formation of the combs, where anomalous dispersion is required to initiate the process. Methods allowing to reliably retrieve the GVD from manufactured devices are then crucial, as to provide fully informed feedback to the design flow step.

Among different techniques, optical frequency domain reflectometry (OFDR) is a well-known interferometric method[4–7] to retrieve the optical amplitude and phase of an optical device under test (DUT). OFDR is preferred among other techniques due to its simpler setup implementation (without requiring mobile parts) and well-balanced characteristics of sensitivity, accuracy, length range and resolution.[6] The technique is increasingly drawing attention in their applications on integrated optics,[8–10] for which its time domain feature with good time/spatial resolution is key to provide the internal full-field structure of the photonic chips.

Previously we reported on the OFDR characterization of the GVD for integrated waveguides in a moderate confinement silicon nitride platform technology.[11,12] In those cases we resolved in time the recirculating contributions of especially designed long MRRs. The method was based on the relative measurement of pulses corresponding to the sequential recirculation in the MRR. Hence, the comparison among internal MRR pulses, allowed to eliminate the instabilities on the measurement set up, leading to a self-calibrated strategy to extract the GVD of the waveguide forming the MRR. In the present work, we employ the same procedure but over high-Q MRR devices instead, which are designed for frequency comb generation. With respect to our previous work, the present measurements are more challenging task due to: a) the impulsive response consists of a very long train of pulses/ time contributions with very low power due to the low coupling regime, and b) the GVD differences between adjacent time contributions are smaller, since short MRRs with low dispersion waveguides are designed. Compared to our previous work, here we propose new approaches to reduce the impact of the measurement noise in order to determine the GVD, as well as to estimate the losses and the coupling regime

Further author information: (Send correspondence to P.M.)
P.M.: E-mail: pascual.munoz@upv.es, Telephone: +34 608 255 449

of the MRR (for an alternative method to retrieve GVD in high-Q MRRs see Ref. 3). Additionally, the group index for the propagating mode in the working bandwidth is also estimated.

The paper is structured as follows: in Section 2 we review the OFDR technique, and elaborate on how the dispersion parameters can be obtained taking advantage of the optical cavity contributions in the time domain. In section 3 we introduce our experimental configuration and results, firstly on the GVD estimation for the different MRR samples and secondly, on the determination of the MRR intrinsic losses and coupling parameters. Finally, the conclusion is presented in Section 4.

2. OFDR AND DISPERSION FROM OPTICAL CAVITIES

OFDR is an homodyne interferometric technique providing extremely useful information of both amplitude and phase in the frequency and time domain. In Fig. 1 a sketch of an OFDR setup is represented. A continuous tunable laser source (TLS) is fed into two Mach-Zehnder interferometers (MZIs). The upper interferometer (DUT-MZI) is used to hold the device under test (DUT) in the upper arm. The beating with the reference arm below generates an interferogram that is suitably sampled by points given by the second MZI (trigger MZI, TRIG-MZI). This allows later on to correct scanning imperfections on the continuous tuning of the TLS. Hence, and after proper sampling the DUT-MZI interferogram, applying the Inverse Fast Fourier Transform (IFFT) results into the corresponding time domain impulse response for the DUT, where the different events can be isolated and bandpass filtered back to the frequency domain. In the setup, the path length differences of both DUT-MZI and TRIG-MZI (ΔL and $\Delta L'$ respectively) are engineered to provide a suitable desired time window specific to the DUT events, i.e. to make the DUT response meet the Nyquist sampling criterion to avoid aliasing in the digital processing.

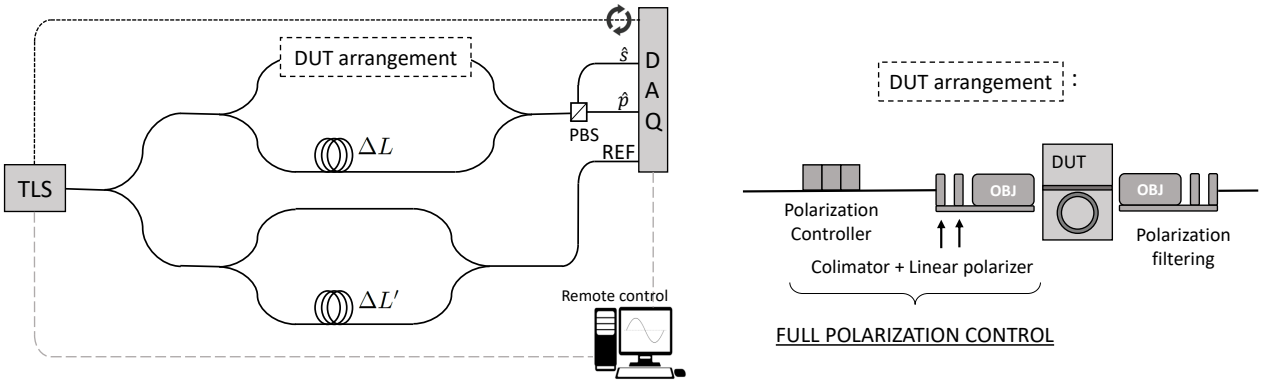

Figure 1. OFDR setup sketch (left), where the TLS feeds both MZIs, the DUT-MZI provides the interferogram containing the DUT response and the proper set of sampling points is dictated by the TRIG-MZI, in a homodyne detection scheme. The DUT arrangement employed (right) for the measurements in this work.

Once in the time-domain, the existing phase information on the DUT impulsive response can be processed, in our case for the MRRs, by using the multiple sequential time contributions of the optical cavity. Hence, the purpose is to obtain the phase evolution, from the consecutive pulses coming from the MRR, in a differential way by explicitly subtracting them. Since internal pulses are used, the unwanted contribution to the measured phase from the setup is cancelled, and only the phase difference between two consecutive (or not) resonant peaks is left. This principle can be applied to MRRs to work out the GVD through the dispersion parameter D*. By knowing the designed round-trip length, every time resolvable contribution can be isolated and independent combinations of them (by pairs) will result into different measurements of the accumulated phase for the given length increment, due to the presence of dispersion on the waveguides.

*Let the reader note that we refer to GVD and D parameter (well-known related by $D = -\frac{2\pi c}{\lambda^2}\beta_2$, where β_2 is the GVD) indistinctly along the paper. The obtained results are though presented as D parameter in units of [ps/(nm*m)]

3. EXPERIMENT

For the experiments, the OFDR setup described in previous section is employed, with a TLS set to 1550 nm center wavelength and 80 nm span, at a scanning speed of 20 nm/s, fed through both the DUT-MZI and the TRIG-MZI. As detailed in Fig. 1 right, polarization control is enforced by means of a fiber polarization controller preceding the fiber collimator, followed by a linear polarizer, just before the focusing objective used to couple light through the edge of the photonic chip. Fiber couplers / combiners are employed as well in the setup, as shown in the figure. The interferograms resulting from the TLS scanning through the MZIs are photodetected by PIN (InGaAs) photodiodes, digitized with a digital acquisition card (DAQ) at 100 kS/s rate, and stored for post-processing. As shown in Fig. 1, a polarization beam splitter is also employed to circumvent the unwanted polarization instabilities in the fiber setup, that cause signal fadings (c.f. Ref. 6).

Regarding the samples, two different MRRs with circular shape of radius $R = 80\,\mu$m where designed and fabricated. The MRRs are coupled to a bus straight waveguide by the evanescent field of the ring/straight waveguides. The two samples differ on the gap between the straight bus waveguide and the MRR, so we refer to them as gap 1 (467 nm) and gap 2 (517 nm). The designed height and width of MRR waveguides are 645 nm and 1650 nm respectively, targeting for anomalous dispersion in optical telecommunication C-band for the TE mode. However, the waveguide width in the MRRs after fabrication was 1570 nm due to some dimension loss. The height and width of the bus straight waveguides are 645 nm and 1000 nm. As for the fabrication process, it was very similar to our previous work in Ref. 13, but using SiH_2Cl_2: $NH_3 = 3.9$ instead. Scanning Electron Microscope (SEM) images of the one of the fabricated samples, prior to cladding deposition, is provided in Fig. 2.

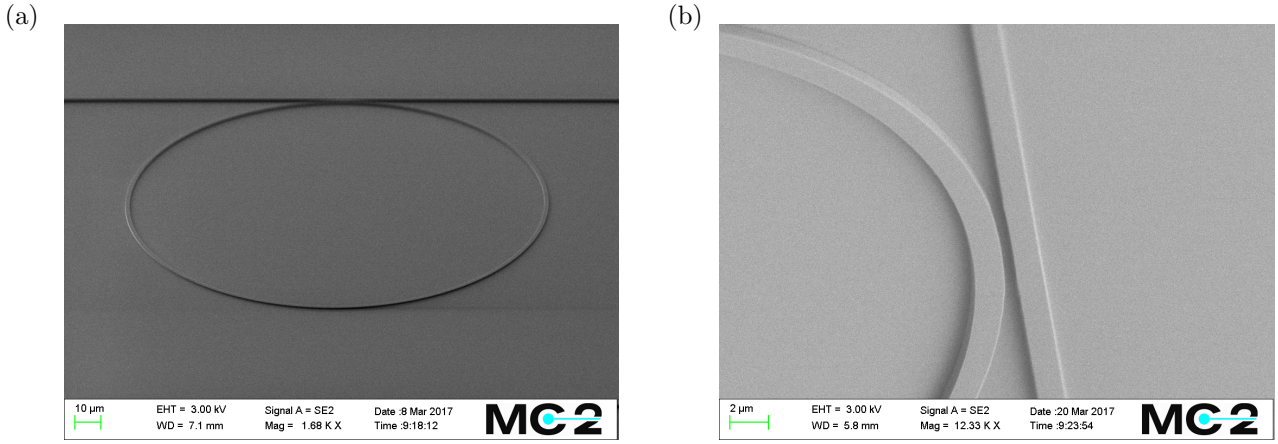

Figure 2. SEM image for one of the MRR samples (a) and close up view of the ring to bus waveguide section (b) prior to cladding deposition.

3.1 DISPERSION

The OFDR measurements were performed for different combinations of the input and output polarizers. Among them, the best resolvable impulse response was observed for TM excitation and TM filtered output. This is in agreement with simulations, wehre the TE is shown to be not coupled to the ring, after the dimensional loss from fabrication. Hence, for TM-TM, we performed measurements corresponding to the aforementioned gap 1 and gap 2 MRRs.

In Fig. 3(a) the obtained time domain response of gap 1 MRR is shown, exhibiting a large number of recirculation pulses well defined over the noise floor. The direct contribution from the straight bus waveguide (the highest) is also appreciated. Furthermore, the peak corresponding to the facet to facet Fabry-Perot (the second highest) can be observed as well. From the time difference between the pulses $\tau = 3.74$ ps and the known MRR (round-trip) length ($2\pi R$), the average group index for the TM mode of the MRR waveguides is $n_g^{TM} = 2.23$. In green, a first set of $M = 30$ consecutive pulses (22 to 51) are isolated to be compared later on with pulses separated $N = 60\times$round-trip times (pulses 82 to 111 in the sequence).

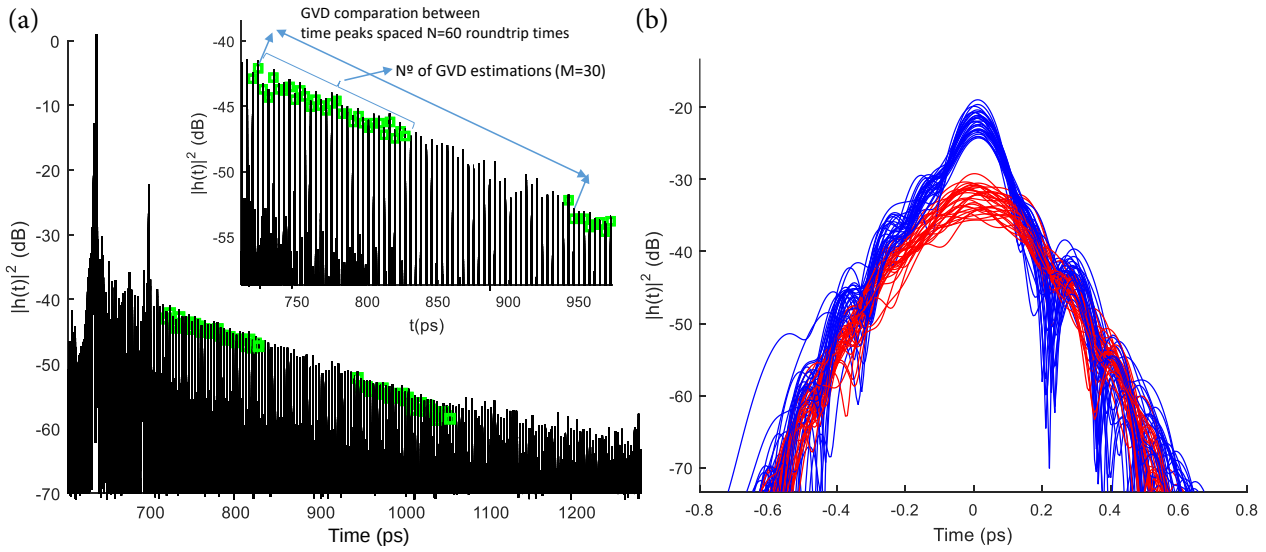

Figure 3. (a) Time domain response of gap 1 MRR, where multiple round-trip contributions can be seen. Labeled in green, pulses that are selected to be truncated are filtered and shown together in (b), the first set in blue and the second one in red.

The isolated pulses are then truncated over a given time range. They are all shown together in Fig. 3(b), the first set in blue and the second one in red, where the slight degradation due to accumulated dispersion can already be appreciated. When truncating single round-trip contributions there is a tradeoff between artificial Group Delay (GD) distortion and the effect of the noise floor. A Gaussian window is applied to reduce the noise, but an excessive time truncation leads to artificial distortion of the GD curve resulting from the FFT, therefore introducing errors in the estimation of the GVD. A compromise value of 0.8 ps (Gaussian window width) was then chosen for these samples. After performing the FFT of the selected band-pass filtered pulses, their GD is obtained by differentiating the optical phase with respect to the angular frequency ω along the measured ω range. Then, the GD traces of the pulses are subtracted to obtain the differential GD, and from it the GVD is derived through a linear fitting procedure. The differential GD between the selected pulse-pairs for the GVD calculation produces the expected linear trend, but with oscillations due to the aforementioned causes, that influence the quality of to the linear fitting process, and gives some uncertainty in the resulting GVD value. In this case we averaged the GVD obtained for the $N = 30$ pulse-pairs processed, in a chosen 'safe' wavelength range of [1540, 1570] nm, as shown if Fig. 4(a). The availability of multiple pulse-pairs allows to reduce the uncertainty by averaging the fitted GVD value as shown in Fig. 4(b)), where the obtained average D is also given along with the corresponding standard deviation σ.

The same procedure has been also applied to the analysis of gap 2 MRRs. In this case, the plotted time domain response in Fig. 5(a) shows the recirculation peaks closer to noise floor in comparison to gap 1 samples, with a dynamic range about 10 dB lower. This is in agreement with a larger gap, corresponding to a to weaker coupling condition. In this case, the second contribution from the facets reflections hampers in the selection of pulses to be processed for GVD estimation as described previously. For this gap 2 MRRs, the first set of pulses starts just after the second facet reflection and a lower separation ($N = 30$) and number of pulse pairs ($M = 20$) can be selected, since the noise floor prevents extending the time range further. Proceeding similarly as described for gap 1 MRR, the set of differential GDs are shown in Fig. 5(b), and the resulting estimations for the GVD by linear fitting are given in Fig. 5(a) as well as an inset.

A summary of the results is provided in Table 1 for the GVD values and associated standard deviations σ. The differences for the three first GVD measurements of gap 1 MRRs are in the order 0.008 ps/(nm*m), corresponding to a relative $\approx 5\%$ error. The two available GVD measurements for gap 2 MRRs show larger

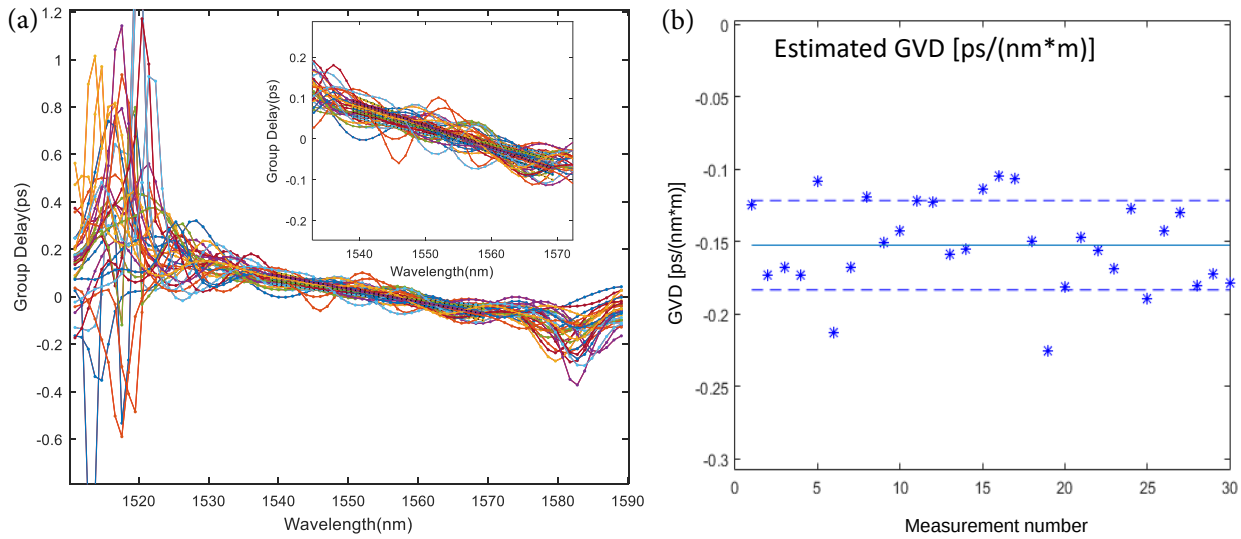

Figure 4. Differential GD (a) for the selected pulse-pairs for gap 1 measurements. In the inset, a zoom of the chosen fitting range for the GVD estimation is shown, with the results plotted in (b), where the average D and the corresponding $\pm\sigma$ (standard deviation) are traced in continuous and dashed lines, respectively.

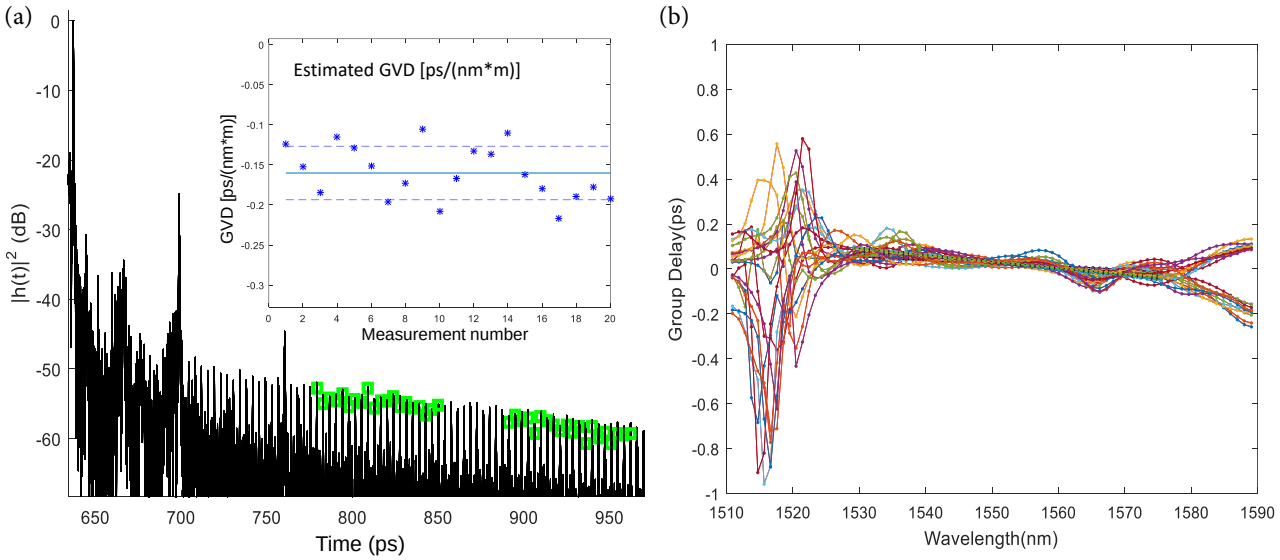

Figure 5. Time domain response (a) of gap 2 MRR, where multiple round-trip contributions can be appreciated. Labeled in green, the selected set of pulses for GVD estimation. In the inset, different GVD estimations calculated by fitting differential GDs shown in (b).

difference. The fourth measurement for gap 1 has been performed for $N = 40$, giving a GVD estimation slightly away from the others. This result, along with the fact the estimations for gap 2 are around the values for gap 1 (as expected, since the waveguide cross-section within the ring is the same), suggests the higher reliability onto the measurements for the first device, which showed contributions further away from noise floor when still keeping to $N = 60$ (where accumulated dispersion is higher and then better resolved). Mode solver simulations (with COMSOL Multi-Physics software) confirm the measurements, yielding an average value of $D = -0.137$ ps/(nm*m) for the range where we have fitted the measurements and derived the GVD values. This in turn provides a good general agreement between the estimated GVD from measurements of this method and the

numerical simulation.

Table 1. Different measurement results for D parameter, for both gap 1 and gap 2 MRRs

Device	# Measurement	D [ps/(nm*m)]	σ [ps/(nm*m)]
gap 1	1	-0.145	0.051
	2	-0.153	0.031
	3	-0.150	0.045
	4	-0.164	0.050
gap 2	1	-0.160	0.034
	2	-0.137	0.027

Finally, we took advantage of the presence of the two spurious chip facet reflections in gap 2 measurements to estimate the D parameter corresponding to the straight bus waveguide. The procedure is the same as above, but with only two pulse contributions, yielding a value of $D = -0.274$ ps/(nm*m). This slightly different dispersion in the straight waveguide, compared to the waveguides forming the MRR cavity is attributed to the different waveguide width, 1000 nm for the bus straight, and 1570 nm for the MRR waveguide.

3.2 COUPLING COEFFICIENT AND INTRINSIC LOSSES

The time domain response of the DUT provides also valuable information about the optical power evolution of the multiple time contributions, that can be used to fit the known response from theoretical models.[14] Hence, the total internal losses and the coupling between the bus and the MRR, can be estimated as well.

Fig. 6(a) shows the complete time domain response normalized in amplitude to the main pulse in time, which as discussed previously corresponds to the direct bus straight waveguide contribution (from input to output of the chip). The normalization to this time contribution removes the total in/out coupling losses to the chip leading to a relative (dB) vertical axis. This is just only related to the cavity evanescent coupling k and its associated losses $(1-\gamma)$, and the ring internal propagation losses L_{RR}. Let the reader find contained in Fig. 6(a) a schematic description and formulae for the power contributions corresponding to sequential pulses in the MRR.

In order to properly extract these parameters we start from the 'raw' OFDR trace depicted in Fig. 6(a). Observe that the pulse amplitude distribution deviates from the expected linear decay dictated by complete round-trip along the ring given by $10\log\left((1-k)\,(1-\gamma)\,L_{RR}\right)$. The discrepancy is due to the pulse distortion effects of the GVD (pulse temporal broadening) over multiple time spans. Notice that the measurements are made along a 80 nm range leading to input equivalent time pulses of ~ 0.1 ps (see Fig. 3 (b)) which are sensitive even to low GVD. To remove this effect, we integrated the total energy contained around the time center of each pulse, in a time interval of $\sim 1-2$ ps, leading to a more uniformly decaying evolution. This way, the effect of dispersion was compensated and only the decay due to loss (coupling and propagation losses) was left. Fig. 6(b) shows the measured peak power (green squares), and the corrected after integration (red dots).

This way, fitting to the theoretical model of the MRR with the compensated peak values (red dots) is done. Firstly, we find the second contribution in time (depicted in Fig. 6(b) as $P[2]$) to compare it with the main contribution $P[1]$ (0 dB in our normalized scale) to obtain the relation: $(P[2]-P[1])\,(\mathrm{dB}) = 10\log\left(\frac{k^2}{1-k}\,(1-\gamma)\,L_{RR}\right)$. Secondly, we proceed with a linear fitting (dotted line) for the corrected time contributions, along the available time range free from spurious, and well over the noise floor noise. Reflections on facets were localized and excluded properly. By using the two previous expressions one can obtain the coupling and losses, that for the shown device (gap 1) are $k = 0.011$ and $(1-\gamma)\,L_{RR} = 0.987$. Additionally, the processing of the approximately ~ 130 pulses yield an average round-trip time of $\tau = 3.74$ ps.

The inset in Fig. 6(a) shows the simulated spectral response employing the analytical expression for the ring resonator[14] and the estimated values as dicussed. We can see a free spectral range of 267.7 GHz (~ 2.2 nm) and 8.2 pm of -3 dB notch bandwidth that agree with the acquired spectral traces.

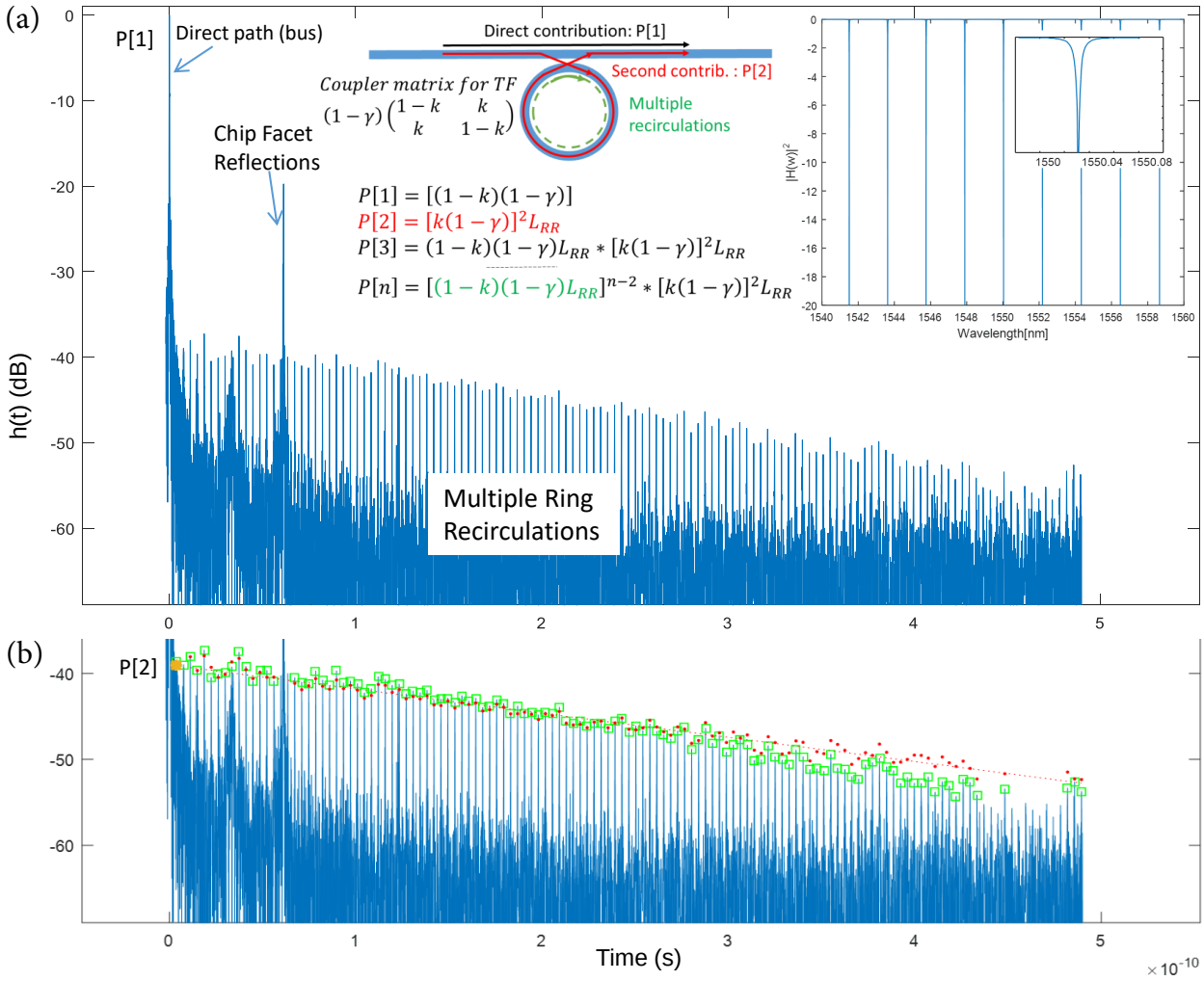

Figure 6. Time response measured for the gap 1 MRR superimposed to the fitted analytical model. The right inset shows a zoomed over a range for some pulse contributions, for both the measurement and the analytical model as well. The left inset provides the reconstruction of the spectral response -with sharp notches- provided by the analytical model.

4. CONCLUSION

In this paper we have reported the use of OFDR measurement techniques for the measurement of high-Q silicon nitride MRR, and described the processes to estimate multiple parameters such as the GVD, critical in the context of non-linear applications, as well as the intrinsic loss, coupling coefficient and group index. The results derived from the measurements are in good agreement with the design and the simulated parameters. The time domain response is shown to be useful in order to localize and analyze internal chip events events, such as the pulses from the natural Fabry-Perot cavity formed by the chip facets.

5. ACKOWNLEDGEMENTS

P.M., D.P. and L.A.B. acknowledge financial support through projects, TEC2015-69787-REDT PIC4TB, TEC2016-80385-P SINXPECT and GVA PROMETEO 2017/103. L.A.B. also acknowledges PTA2015-11309-I. Z.Y. acknowledge financial support by the Swedish research council (VR).

REFERENCES

[1] Levy, J. S., Gondarenko, A., Foster, M. A., Turner-Foster, A. C., Gaeta, A. L., and Lipson, M., "Cmos-compatible multiple-wavelength oscillator for on-chip optical interconnects," *Nature Photonics* **4**, 37–40 (2010).

[2] Papp, S. B., Beha, K., Del'Haye, P., Quinlan, F., Lee, H., Vahala, K. J., and Diddams, S. A., "Microresonator frequency comb optical clock," *Optica* **1**(1), 10–14 (2014).

[3] Zhu, J., Ozdemir, S. K., Xiao, Y.-F., Li, L., He, L., Chen, D.-R., and Yang, L., "On-chip single nanoparticle detection and sizing by mode splitting in an ultrahigh-q microresonator," *Nature Photonics* **4**, 46 (2009).

[4] Eickhoff, W. and Ulrich, R., "Optical frequency domain reflectometry in singlemode fiber," *Applied Physics Letters* **39**(9), 693–695 (1981).

[5] Glombitza, U. and E., B., "Coherent frequency-domain reflectometry for characterization of single-mode integrated-optical waveguides," *IEEE Journal of Lightwave Technology* **11**, 1377 – 1384 (Aug. 1993).

[6] Soller, B. J., Gifford, D. K., Wolfe, M. S., and Froggatt, M. E., "High resolution optical frequency domain reflectometry for characterization of components and assemblies," *Opt. Express* **13**, 666–674 (Jan 2005).

[7] Gifford, D. K., Soller, B. J., Wolfe, M. S., and Froggatt, M. E., "Optical vector network analyzer for single-scan measurements of loss, group delay, and polarization mode dispersion," *Appl. Opt.* **44**, 7282–7286 (Dec 2005).

[8] Bru, L. A., Gargallo, B., Micó, G., Baños, R., Doménech, J. D., Sánchez, A. M., Mas, R., Pardo, E., Pastor, D., and Muñoz, P., "Optical frequency domain reflectometry applied to photonic integrated circuits," in [*European Conference on Integrated Optics (ECIO) 2016 proceedings*], paper o–08 (May 2016).

[9] Melati, D., *A design kit perspective in InP-based photonic integrated circuits*, PhD thesis, Polytechnic University of Milan (2014).

[10] Zhao, D., Pustakhod, D., Williams, K., and Leijtens, X., "High resolution optical frequency domain reflectometry for analyzing intra-chip reflections," *IEEE Photonics Technology Letters* **29**, 1379–1382 (Aug. 2017).

[11] Bru, L. A., Micó, G., Pastor, D., Doménech, D., Sánchez, A. M., Cirera, J. M., Sánchez, J., Domínguez, C., and Muñoz, P., "Full field group velocity dispersion characterization of 300nm film height silicon nitride waveguides," in [*European Conference on Integrated Optics (ECIO) 2017 proceedings*], MP1.4 (Apr. 2017).

[12] Muñoz, P., Micó, G., Bru, L. A., Pastor, D., Pérez, D., Doménech, J. D., Fernández, J., Baños, R., Gargallo, B., Alemany, R., Sánchez, A. M., Cirera, J. M., Mas, R., and Domínguez, C., "Silicon nitride photonic integration platforms for visible, near-infrared and mid-infrared applications," *Sensors* **17**(9), 2088 (2017).

[13] Krückel, C. J., Fülöp, A., Klintberg, T., Bengtsson, J., Andrekson, P. A., and Torres-Company, V., "Linear and nonlinear characterization of low-stress high-confinement silicon-rich nitride waveguides," *Opt. Express* **23**, 25827–25837 (Oct 2015).

[14] Madsen, C. K. and Zhao, J. H., [*Optical Filter Design and Analysis: A Signal Processing Approach*], John Wiley & Sons, Inc. (1999).